Decadal variability of northern northeast Brazil rainfall and its relation to tropical sea surface temperature and global sea level pressure anomalies

Mary Toshie Kayano and Rita Valéria Andreoli

Centro de Previsao de Tempo e Estudos Climaticos, Instituto Nacional de Pesquisas Espaciais, São Paulo, Brazil

Received 12 April 2004; revised 26 August 2004; accepted 16 September 2004; published 19 November 2004.

[1] Decadal (9–14 year) relations of the northern northeastern Brazil (NEB) rainfall to the sea surface temperature (SST) in the 60°N–30°S oceanic sector and to the global sea level pressure (SLP) anomalies are investigated for the 1871–1991 period. Indices are defined for the precipitation and for the SST anomalies in the tropical North Atlantic (TNA), in the tropical South Atlantic (TSA), and in the eastern equatorial Pacific (T-TNA, T-TSA, and T-NINO indices, respectively). An index is also defined for the SLP anomalies in the North Atlantic Oscillation region (P-NAO index). These indices and the SST and SLP anomaly time series are filtered for the decadal scale using the continuous wavelet transform. The filtered time series are then subjected to the correlation and partial correlation analyses. The results indicate that the decadal variations of the northern NEB rainfall might be independently linked to the Pacific Decadal Oscillation (PDO)/NAO/TNA decadal relations or to the SST decadal variations in the TSA. This is a new result not discussed before. The northern NEB rainfall linkage to the PDO/NAO/TNA relations is indicative that the relationship of the SLP variations in the NAO region and the NEB rainfall proposed in a work during the 1970s is part of the decadal climate variability that connects the PDO in the tropical Pacific to the NEB rainfall through the Northern Hemisphere extratropical atmosphere. *INDEX TERMS:* 1635 Global Change: Oceans (4203); 3339 Meteorology and Atmospheric Dynamics: Ocean/atmosphere interactions (0312, 4504); 3354 Meteorology and Atmospheric Dynamics: Precipitation (1854); 3374 Meteorology and Atmospheric Dynamics: Tropical meteorology; *KEYWORDS:* decadal variability, northeast Brazil, precipitation

Citation: Kayano, M. T., and R. V. Andreoli (2004), Decadal variability of northern northeast Brazil rainfall and its relation to tropical sea surface temperature and global sea level pressure anomalies, *J. Geophys. Res.*, *109*, C11011, doi:10.1029/2004JC002429.

1. Introduction

[2] It is well known that the El Niño–Southern Oscillation (ENSO) in the tropical Pacific is one of the major remote phenomena causing significant climate variations in the northeast Brazil (NEB). The ENSO connection to the NEB climate occurs through the atmospheric circulation in such a way that an El Niño–related drought is attributed to an eastward displaced Walker circulation with anomalous rising motion (enhanced convection) over the eastern equatorial Pacific and sinking motion (inhibited convection) further east over the tropical Atlantic [*Hastenrath*, 1976; *Kousky et al.*, 1984; *Kayano et al.*, 1988; *Ropelewski and Halpert*, 1987, 1989; *Kiladis and Diaz*, 1989; *Rao and Hada*, 1990]. Nearly reversed anomalous patterns of the atmospheric circulation, sea surface temperature (SST), and NEB rainfall are observed during La Niña episodes [*Kousky and Ropelewski*, 1989].

[3] Recent studies have found another mode of the SST variability in the Pacific, similar to the ENSO, with significant climate teleconnections but varying at a decadal scale [*Nitta and Yamada*, 1989; *Zhang et al.*, 1997; *Mantua et al.*, 1997; *Zhang et al.*, 1998] (hereinafter referred to as the Pacific Decadal Oscillation (PDO)). The global SST, sea level pressure (SLP), and wind stress anomaly patterns for the PDO and ENSO modes are similar; however, the PDO pattern for the SST is less equatorially confined in the eastern Pacific and more prominent in the extratropical North Pacific [e.g., *Zhang et al.*, 1997]. The PDO-related 500 hPa height field for the boreal winter resembles the Pacific/North America (PNA) pattern [*Zhang et al.*, 1997] that was previously identified as a teleconnection pattern from a correlation analysis for 15 winters by *Wallace and Gutzler* [1981]. In the Atlantic the SLP anomaly structure associated with the PDO mode resembles the North Atlantic Oscillation (NAO) pattern [*Mo and Häkkinen*, 2001], which was first identified as a teleconnection pattern by *Walker and Bliss* [1932]. In this work the high (low) PDO phase will be referred to the SST anomaly pattern characterized by warm (cold) waters in the central and eastern tropical Pacific.

[4] Several authors have shown linkages between the NAO-associated circulations and the tropical Atlantic SST anomalies at the decadal scale [*Rajagopalan et al.*, 1998;

0148-0227/04/2004JC002429$09.00

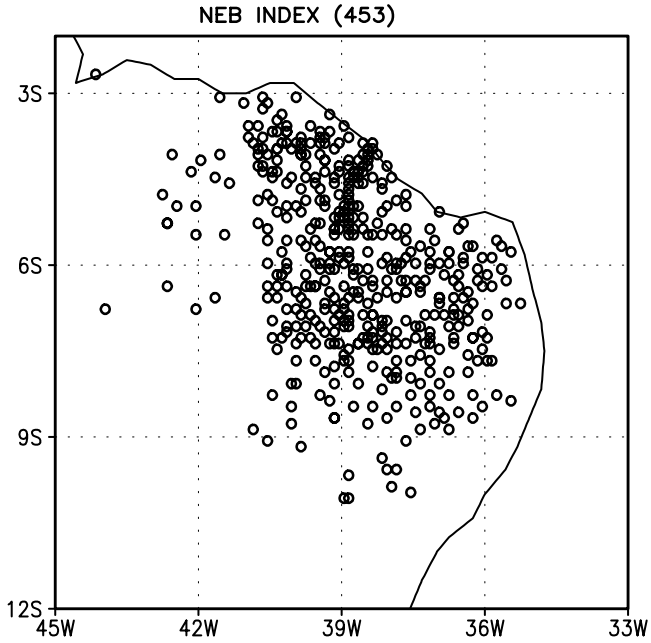

Figure 1. Locations of the rainfall stations.

Xie and Tanimoto, 1998; *Tanimoto and Xie*, 1999; *Häkkinen and Mo*, 2002]. However, for the decadal scale, the dominant SST anomaly pattern in the tropical Atlantic features a cross-equatorial SST anomaly gradient mode (SST gradient mode) [e.g., *Mehta*, 1998; *Mehta and Delworth*, 1995; *Tourre et al.*, 1999; *Andreoli and Kayano*, 2003]. This mode relates hydrostatically to the SLP and wind patterns over the equatorial Atlantic and affects the meridional displacements of the Intertropical Convergence Zone (ITCZ) [*Hastenrath and Greischar*, 1993; *Nobre and Shukla*, 1996]. The southward (northward) SST anomaly gradient relates to an anomalously southward (northward) displaced Atlantic ITCZ that leads to a wetter (drier) than normal NEB rainy season [e.g., *Hastenrath and Heller*, 1977; *Moura and Shukla*, 1981; *Hastenrath and Greischar*, 1993; *Nobre and Shukla*, 1996].

[5] Earlier studies have associated the NEB rainfall variations with the PNA and NAO patterns [*Rao and Brito*, 1985; *Namias*, 1972]. *Rao and Brito* [1985], correlating the northern winter geopotential heights at 700 hPa and March rainfall over the NEB, found a correlation pattern similar to the PNA. They interpreted the PNA pattern as a link between the NEB rainfall and the Northern Hemisphere (NH) winter circulation through the ENSO. *Namias* [1972] related the droughts (floods) in the northern NEB to weakened (strengthened) cyclonic activity in Greenland area and anticyclonic activity in the Azores region, through the associated changes in the subtropical North Atlantic anticyclone and in the northeast trade winds. The circulation anomalies obtained by *Namias* [1972] resembles the NAO teleconnection pattern.

[6] The results above suggest decadal relations between the PDO and NAO modes and between the NAO mode and the tropical Atlantic SST anomaly modes. How these modes are related to the rainfall variations in the NEB for the decadal scale was not investigated before. So the present work focuses directly on the decadal relations of NEB rainfall to SST variations in the tropical oceans and to global SLP variations using wavelet analysis and correlation and partial correlation techniques.

2. Data and Methodology

[7] The data used are global monthly SST anomalies and SLP gridded on a 5° by 5° latitude-longitude resolution and the monthly precipitation of Fortaleza (3°47′S, 38°32′W) over the 1871–1991 period. The SST data consist of the *Kaplan et al.* [1998] reanalysis of the UK Meteorological Office Global Ocean Surface Temperature Atlas for the SST. The SLP data are obtained from the British Atmospheric Data Centre at the following Web page: http://www.badc.rl.ac.uk/. Roberto L. Guedes from the Centro Técnico Aeroespacial kindly provided the precipitation time series. Part of this series from 1871 to 1970 was extracted from *Strang* [1972].

[8] In addition, monthly precipitation data of 453 rainfall stations in the NEB, all of them located north of 10°S (Figure 1) and ~11% of them spanning from 1911 to 1990, are also used. These data, kindly provided by José I. B. de Brito from the Universidade de Campina Grande, were obtained from several sources, including the Superintendência do Desenvolvimento do Nordeste, the Departamento Nacional de Obras contra a Seca, and the Fundação Cearense de Meteorologia e Recursos Hídricos. It is worth mentioning that the 453 rainfall stations, selected from a more numerous data set, are those with at least 30 years of information and with the rainiest 3 months from February to April or from March to May. Before these data are used, they are checked for errors. Monthly standard deviations are calculated for each time series, and any monthly value higher than three standard deviations is replaced by the missing data code. Finally, the monthly rainfall data are used to obtain an area-averaged NEB rainfall index (NEB index) for the 1911–1990 period.

[9] The analyses using the SST data are constrained to the 60°N–30°S band, mainly because of the sparse data coverage south of 30°S. Monthly anomalies are computed for the SLP time series at each grid point, for Fortaleza precipitation time series as departures from the 1871–1991 base period means, and for the NEB index from the 1911–1990 base period means.

[10] The SST indices (averaged SST anomalies) are defined for tropical areas with dominant SST anomaly patterns, which are bounded at 2.5°N, 22.5°N, 67.5°W, and 27.5°W for the TNA (T-TNA index); at 2.5°N, 17.5°S, 32.5°W, and 12.5°E for the TSA (T-TSA index); and at 5°N, 5°S, 150°W, and 90°W for the eastern equatorial Pacific (T-NINO index). The T-NINO index is indeed the SST index in the Niño-3 region. Fortaleza precipitation anomaly time series is used as an index (PRP index) to represent the rainfall variations in the northern NEB. This is justified by the fact that the rainfall variability in this sector has quite homogeneous signature [*Kousky and Chu*, 1978; *Aceituno*, 1988; *Kayano et al.*, 1988; *Ropelewski and Halpert*, 1987, 1989; *Kane and Trivedi*, 1988]. *Kane and Trivedi* [1988], using rainfall data for stations in the NEB for the 1915–1978 period, showed that Fortaleza is positively correlated with the stations located north of 10°S. They found correlations higher than 0.6 for most stations

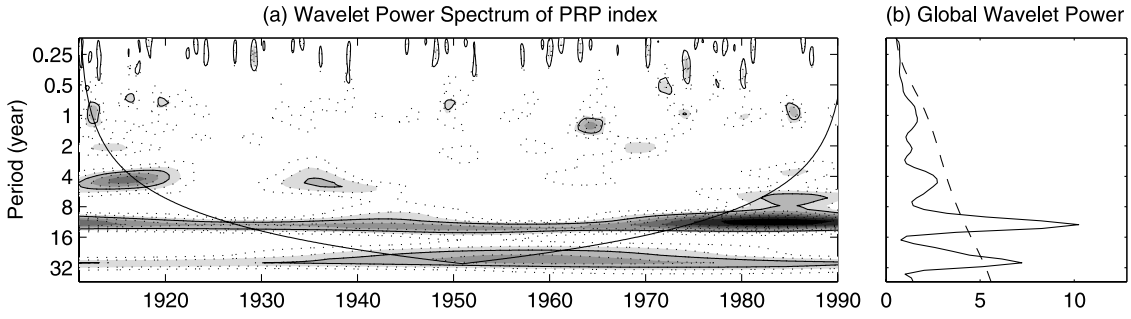

Figure 2. (a) Local wavelet power spectrum (power) of the continuous wavelet transform (CWT) of the PRP index normalized by the $1/\sigma^2$ ($\sigma^2 = 8.6 \times 10^3$ mm^2) and (b) GWS in variance units. Shaded contours in Figure 2a are normalized power varying from 2 to 16 with interval of 2. Closed contours in Figure 2a encompass significant power at 95%. Region where the edge effects are important is under the U-shaped curve in Figure 2a, and therefore the power in this region is not considered in the analysis. Dashed curve in Figure 2b is the 95% confidence level for the GWS, assuming a red noise spectrum.

north of 8°S. The PRP and NEB indices are subject to the wavelet analysis in order to compare their frequency-time variation features.

[11] Monthly raw index for the NAO, based on the difference in the SLP between Ponta Delgada, Azores (38°N, 26°W), and Akureyri, Iceland (66°N, 18°W), for the 1874–1991 period defined by *Rogers* [1984] and available at http://bprc.mps.ohio-state.edu/gpl/NAO is also used. In the present paper this index is referred to as the P-NAO index. Because of its definition, negative (positive) P-NAO index, or equivalently negative (positive) phase of the NAO, means weakened (strengthened) cyclonic activity in Iceland and anticyclonic activity in the Azores region. Analyses involving the P-NAO index are based on the 1874–1991 period.

[12] A continuous wavelet transform (CWT) is used as a band-pass filter to isolate the decadal oscillations from the time series and to decompose a time series into a time-frequency space [e.g., *Torrence and Compo*, 1998]. The Morlet wavelet, used here, is a complex exponential modulated by a Gaussian, $e^{i\omega_o\eta}e^{-\eta^2}/2$, with $\eta = t/s$, where t is the time, s is the wavelet scale, and ω_0 is a nondimensional frequency. The computational procedure of the wavelet analysis described by *Torrence and Compo* [1998] is used here. The wavelet function at each scale s is normalized by $s^{-1/2}$ to have unit energy, which ensures that the wavelet transform at each scale s is comparable to each other and to the transform of other time series. The wavelet-filtered time series for decadal band (9–14 years) is obtained from *Torrence and Compo* [1998, equation (29)]. Before performing the wavelet analyses, the long-term linear trends are removed from the time series, and the detrended series are normalized by the corresponding standard deviations.

[13] Correlation maps between the PRP index and the SST and SLP anomaly time series are obtained from linear correlation and partial correlation calculations for the decadal scale. Therefore the PRP, P-NAO, and SST indices and the SST and SLP anomaly time series at each grid point are subjected to the filtering procedure. The partial correlation method is used to obtain the decadal relation between the PRP index and the SST and SLP time series while excluding the influences due to the SST indices or to the P-NAO index. The partial correlation between two variables, X_1 and X_3, while excluding the influences of a third independent variable, X_2, is defined as [*Panofsky and Brier*, 1968]

$$r_{13,2} = (r_{13} - r_{12}r_{23}) \Big/ \sqrt{(1 - r_{12}^2)}\sqrt{(1 - r_{23}^2)},$$

where r_{13}, r_{12}, and r_{23} are the linear correlations between X_1 and X_3, between X_1 and X_2, and between X_2 and X_3, respectively. In short words, the linear correlation between X_1 and X_2 is referred to as "$X_1 \times X_2$ correlation," and the partial correlation between X_1 and X_3 without the effects of X_2 is referred to as "$X_1 \times X_3$ minus X_2 partial correlation."

[14] To assess the statistical significance of the correlations, the number of degrees of freedom is estimated using the method of *Zhang and Hendon* [1997]. The result is approximately 8 degrees of freedom, which is the total number of years in a time series (121 years) divided by 14 years (the maximum period considered for the decadal band). Using the Student's t test, it is found that absolute correlations >0.63 are significant at the 95% confidence level. It is worth noting that this is a local correlation significance test and not a field significance test. *Livezey* [1995], discussing this aspect of the significance for the correlation map between the Southern Oscillation index and the 700 hPa heights, showed that 6% of the global area can exceed the 95% confidence level for Student's t test by chance. So, while discussing the correlation maps, only the patterns covering an area larger than 6% of the globe will be considered.

3. Results

3.1. Comparisons Between the NEB and PRP Indices for the 1911–1990 Period

[15] Figures 2 and 3 show the wavelet analyses of the PRP index (Fortaleza) and of the NEB index (area-averaged precipitation over NEB) during 1911–1990. The global wavelet spectrum (GWS) plots of the PRP and NEB indices are displayed in Figures 2b and 3b. It is important to note that the GWS plots of the two indices show similar spectral behavior, which is more conspicuous for the interannual and decadal scales (Figures 2b and 3b). In fact, both Figure 2b

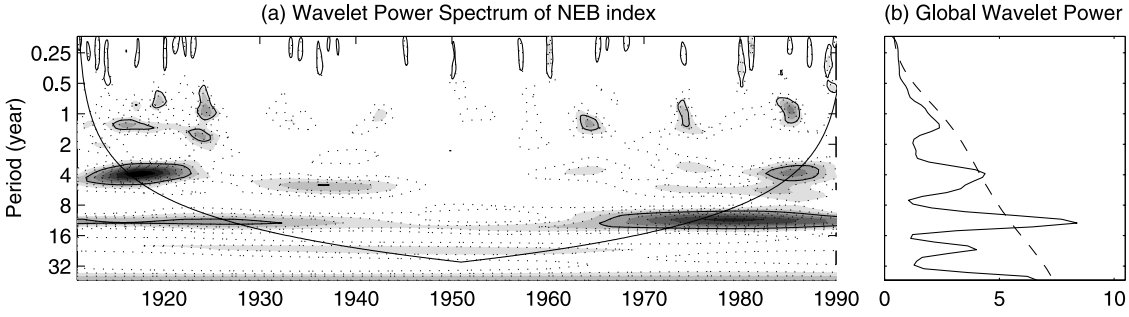

Figure 3. (a) Local wavelet power spectrum (power) of the CWT of the NEB index normalized by the $1/\sigma^2$ ($\sigma^2 = 2.0 \times 10^3$ mm^2) and (b) GWS in variance units. Display is the same as that in Figure 2.

and Figure 3b exhibit the largest GWS values at the decadal scale, which are significant at the 5% level for the interval from 10 to 13 years and peak approximately at 12 years. The GWS plot for the NEB index shows a secondary peak significant at the 5% level at the interannual scale (from 3 to 4 years). The GWS plot for the PRP index also shows a secondary peak at this scale; however, it is nonsignificant. In addition, both plots show a secondary peak at a multidecadal scale (from 26 to 28 years), which is significant for the PRP index and nonsignificant for the NEB index.

[16] The local wavelet power spectra (power) for the two indices, displayed in time period plots (Figures 2a and 3a), also show similarities. The strong decadal peaks in the GWS of the NEB and PRP indices are due to the significant (at the 5% level) decadal power observed during the first 20 years and the last 25 years of the 1911–1990 period. The PRP index shows significant decadal power from 1930 to 1965, whereas the NEB index shows less pronounced decadal power for the same period. The secondary interannual peaks (from 3 to 4 years) in the GWS of the NEB and PRP indices are due to the interannual power observed during the 1911–1920, 1930–1945, 1960–1965, and 1980–1990 periods. For the scales shorter than 1 year and longer than 25 years the local wavelet power spectra of the PRP and NEB indices show some differences, in such a way that the PRP index contains relatively more power than the NEB index for these scales.

[17] The PRP and NEB indices show the largest GWS values at the decadal scale, which are significant at the 5% level for the interval from 10 to 13 years. So the 9–14 year band, which comprises this interval of years, is used for the decadal scale. This band explains 3.4% (3.6%) of the total variance of the PRP (NEB) index. Although this percentage seems to be low, it is relative to the total variance of time series without any filter. Since most of the rainfall in the northern NEB is concentrated in the autumn season, time series with one value per year (the autumn values or annual totals) would be equivalent to the low-pass filtered time series for periods longer than 1 year. For the low-pass filtered NEB and PRP indices, the percentage of the total variance contained in the decadal scale is 10%, which seems a reasonable value.

3.2. Relations Among the Decadal Indices

[18] The linear correlations among the decadal PRP, SST, and P-NAO indices are given in Table 1. The PRP index is significantly correlated with all other indices, being positively correlated with the P-NAO and T-TSA indices and negatively correlated with the T-NINO and T-TNA indices (Table 1). Significant correlations are also found for the following pairs of indices: T-NINO and T-TNA, T-NINO and P-NAO, and T-TNA and P-NAO. Some of these correlations, although statistically significant, may not represent direct physical connection. These are the cases of the T-NINO × T-TNA and P-NAO × PRP correlations.

[19] The significant negative correlation of −0.75 between T-NINO and P-NAO for the decadal scale reinforces previous results on the positive relation between the NAO and ENSO. *Gershunov and Barnett* [1998] suggested that the PDO modulates the ENSO teleconnections, in such a way that the negative (positive) phase of the NAO occurs during the El Niño (La Niña) events, in particular for those observed during the low (high) phase of the PDO.

[20] The significant T-NINO × P-NAO (of −0.75), P-NAO × T-TNA (of −0.77) and T-TNA × PRP (of −0.66) correlations are indicative of a chain of sequential correlations, which may have physical interpretation. In order to illustrate these correlations the T-NINO, P-NAO, T-TNA, and PRP indices are displayed in Figure 4. The negative T-NINO × P-NAO × T-TNA × PRP sequential correlations mean that warm (cold) waters in the eastern tropical Pacific are associated with the negative (positive) phase of the NAO, which is related to positive (negative) SST anomalies in the TNA, which in turn are related to drier (wetter) than normal conditions in the northern NEB, for the decadal scale.

[21] On the other hand, the T-TSA × PRP positive correlation implies that the negative (positive) SST anomalies in the TSA are related to the northern NEB reduced (increased) rainfall. In addition, the T-TSA index exhibits weak relations to the T-NINO, T-TNA, and P-NAO indices. This suggests that the decadal SST variability in the TSA is not driven by SST variations in the eastern equatorial

Table 1. Linear Correlations Among the Decadal PRP, T-NINO, T-TNA, T-TSA, and P-NAO Indices[a]

	PRP	T-NINO	T-TNA	T-TSA	P-NAO
PRP	1	−0.65	−0.82	0.71	0.66
T-NINO		1	0.87	−0.25	−0.75
T-TNA			1	−0.35	−0.77
T-TSA				1	0.41
P-NAO					1

[a]Absolute correlations >0.63 are significant at the 95% confidence level.

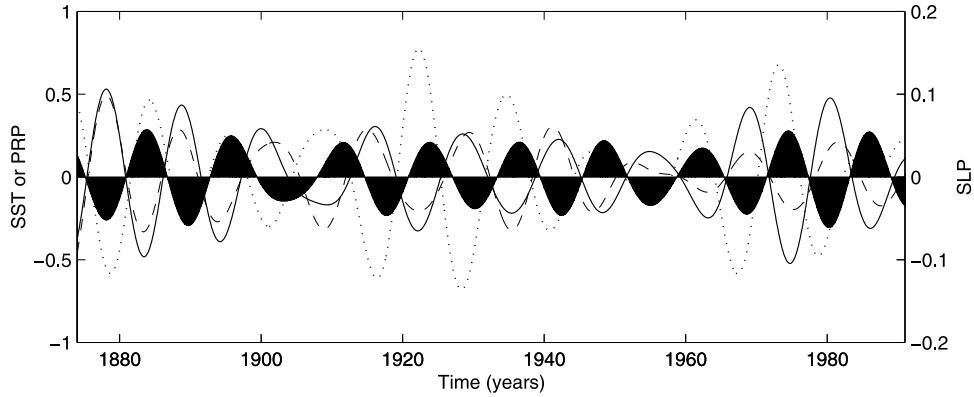

Figure 4. Plots of the decadal T-NINO (dashed curve), decadal T-TNA (solid curve), decadal P-NAO (dotted curve), and decadal PRP (sinusoidal curve contouring the dark areas) normalized indices. Left scale is for the SST and PRP indices, and the right scale is for the P-NAO index.

Pacific and in the TNA or by the SLP variations in the NAO region. It is important to notice that the T-TSA × T-TNA correlation, though negative, is not significant. This implies that although the SST decadal patterns in the TNA and in the TSA might occasionally configure a SST gradient pattern, in general, they do not relate directly to each other, as shown by *Andreoli and Kayano* [2004].

3.3. Correlation Maps

[22] Correlation maps between the rainfall indices and the SST and SLP anomaly time series are calculated for the PRP and NEB indices. Because of the similar features of the correlation maps for these indices and considering that the decadal analysis requires long time series, only the maps for the PRP index (or Fortaleza rainfall time series) are shown and discussed.

[23] The decadal linkages of the PRP index with the other indices, discussed above in section 3.2, are reproduced in the SST × PRP correlation map, which shows significant values in the areas corresponding to these indices (Figure 5). Negative correlations are found in the central and eastern equatorial Pacific and along the western coast of North America, and the positive ones are centered in the North Pacific and surrounding Papua/New Guinea. In the NAO region, negative correlations are observed to the southeast of Greenland, and the positive ones are observed in the western TNA north of 20°N. In the tropical Atlantic, large negative correlations are found in most of the TNA, and the positive correlations are located in the equatorial Atlantic and in the eastern TSA (Figure 5). The correlation pattern in the Pacific resembles the leading decadal PDO mode for the SST previously discussed by *Zhang et al.* [1997], while that in the tropical Atlantic is similar to the SST gradient mode. These results suggest that the PDO mode for the SST in the Pacific and the SST gradient mode in the tropical Atlantic are both closely linked to the rainfall variations in the northern NEB for the decadal scale.

[24] The SLP × PRP correlation map for the decadal scale is shown in Figure 6. Significant negative correlations are found in the equatorial Atlantic and in the eastern TSA, and significant positive correlations are found in the central tropical North Pacific. This map also exhibits significant correlations in the NAO region with negative values over the southeastern Greenland and the adjacent north Atlantic area and the positive ones over the western North Atlantic between 45° and 15°N. The negative correlations in the TSA imply that weakened (strengthened) subtropical South Atlantic high-pressure system is associated with wetter (drier) than normal conditions in the northern NEB. The correlation pattern in the North Atlantic suggests that the relationship of the northern Atlantic SLP variations and the NEB rainfall proposed by *Namias* [1972] is part of the decadal variability. Significant negative correlations are also found in an extensive area including southern India and most of the Indian Ocean north of 30°S. However, these correlations might be part of a complex decadal mechanism connecting Atlantic and Indian circulation. This aspect is out of the scope of the present paper. So these correlations are not interpreted.

[25] The partial correlation maps between the rainfall index and the SST and SLP anomaly time series, while excluding the influence of the SST and P-NAO indices, are also calculated for the PRP and NEB indices. Because of the similar partial correlation maps for both indices and to be consistent with the results above in this section, only the maps for the PRP index are shown.

[26] The SST × PRP minus T-NINO and SST × PRP minus T-TNA partial correlation maps show similar patterns, with significant positive values in the equatorial

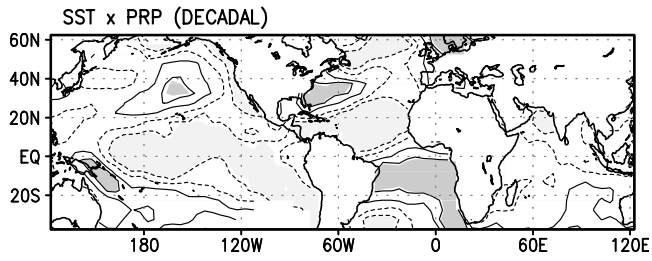

Figure 5. Correlation map obtained by linearly correlating the PRP index and the SST anomaly time series at each grid point for the decadal scale. Contour interval is 0.3. Dark (light) shading indicates values greater (less) than 0.63 (−0.63), which are significant at the 95% confidence level. Zero line is not shown.

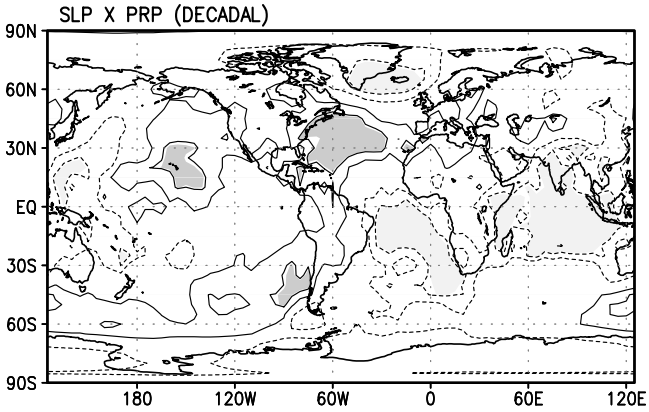

Figure 6. Correlation map obtained by linearly correlating the PRP index and the SLP anomaly time series at each grid point for the decadal scale. Display is the same as that in Figure 5.

Atlantic, in most of the TSA and in the central Indian Ocean. Significant values are also found in small centers aligned in the southeast-northwest direction in the Pacific sector approximately between 150°E and 140°W (Figures 7a and 7b). The SST × PRP minus T-NINO partial correlation map also shows significant negative values in small areas of the Atlantic Ocean north of 10°N. The SST × PRP minus P-NAO partial correlation map (Figure 7c) shows a pattern quite similar to that of the SST × PRP minus T-NINO. Significant positive values are found in the equatorial Atlantic and in the eastern TSA (Figure 7c). So the partial correlation patterns indicate that the positive correlations between the NEB rainfall and the SST anomaly time series in most of the TSA are weakly influenced by the SST variations in the eastern Pacific and in the TNA and by the SLP variations in the NAO region for the decadal scale.

[27] The outstanding feature of the SST × PRP minus T-TSA partial correlation map for the decadal scale is the occurrence of significant negative values in an extensive area including the central and eastern Pacific, the western coast of Central and North America, and the TNA area south of 20°N (Figure 7d). Significant values are also noted surrounding Papua/New Guinea (positive) and in the NAO region. So the negative correlations between the NEB rainfall and the SST anomaly time series in the central and eastern Pacific, in the western coast of Central and North America, and in the TNA are not affected by the SST variations in the TSA for the decadal scale.

[28] The decadal SLP × PRP minus T-NINO and SLP × PRP minus T-TNA partial correlation maps show quite similar features with significant negative values in the eastern TSA and in the central Indian Ocean (Figures 8a and 8b). So the negative relations of the NEB rainfall and the SLP anomalies in the TSA are weakly related to the SST variations in the eastern equatorial Pacific and in the TNA, for the decadal scale. For the same reason given above in this section, the correlations in the Indian Ocean are not interpreted. The decadal SLP × PRP minus P-NAO correlation map (figure not shown), in general, shows very small magnitudes but with correlation signs consistent with those of Figures 8a and 8b. The SLP × PRP minus T-TSA partial correlation map shows significant values in the NAO region (Figure 8c). So the SLP decadal variability in the NAO region associated with the NEB rainfall is not affected by the SST variations in the TSA.

4. Concluding Remarks

[29] The decadal (9–14 year) relations of the northern northeastern Brazil (NEB) rainfall to the sea surface temperature (SST) anomalies in the oceanic sector bounded at 60°N and 30°S and to the global sea level pressure (SLP) anomalies are investigated using correlation and partial correlation analyses for the 1871–1991 period. A careful examination of Table 1 suggests the existence of the physically meaningful sequential correlations which are the T-NINO × P-NAO × T-TNA × PRP. These correlations are all negative and can be interpreted as follows: a warm (cold) PDO mode in the Pacific is accompanied by changes

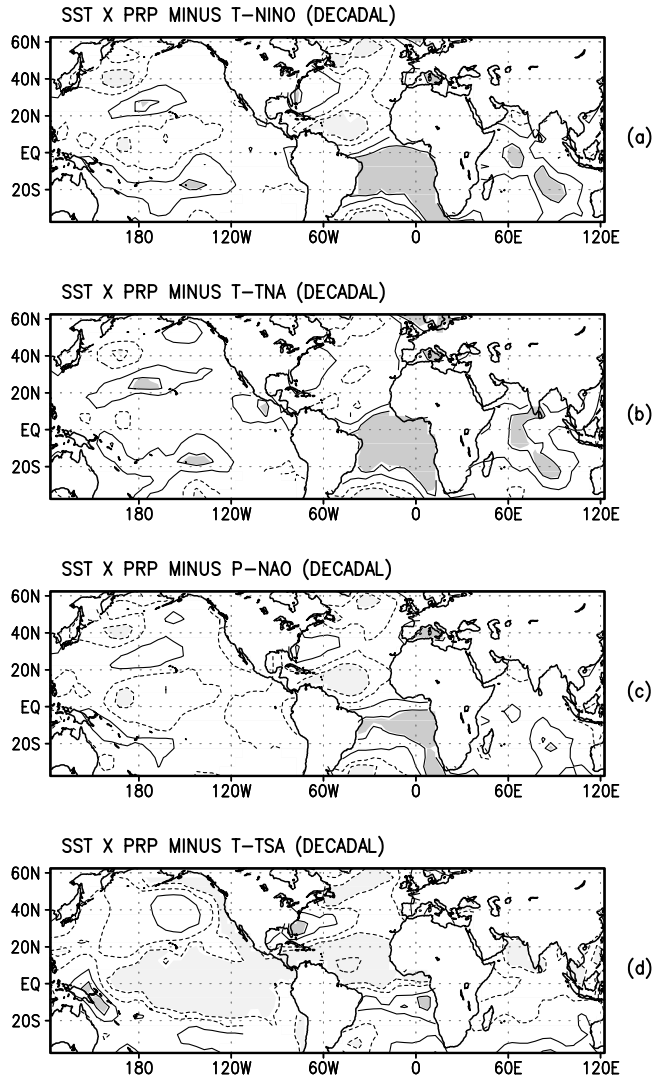

Figure 7. Decadal partial correlation maps obtained by correlating the PRP index and the SST anomaly time series at each grid point while excluding the influence of (a) T-NINO index, (b) T-TNA index, (c) P-NAO index, and (d) T-TSA index. Display is the same as that in Figure 5.

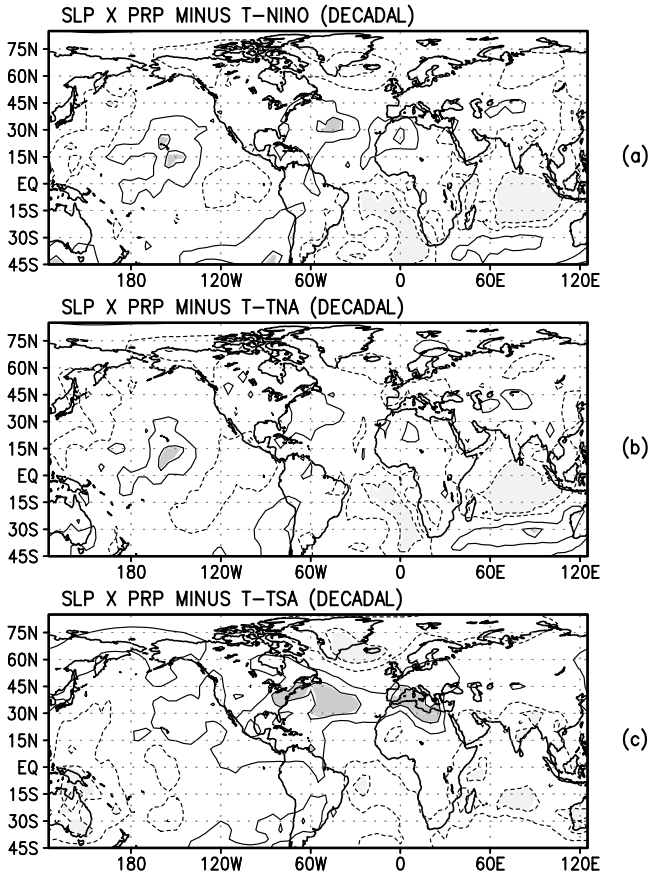

Figure 8. Decadal partial correlation maps obtained by correlating the PRP index and the SLP anomaly time series at each grid point while excluding the influence of (a) T-NINO index, (b) T-TNA index, and (c) T-TSA index. Display is the same as that in Figure 5.

in the NH midlatitude atmospheric circulation, in such a way that a negative- (positive-) phase NAO is established in the North Atlantic region, consistent with *Mo and Häkkinen*'s [2001] findings. Then, this negative- (positive-) phase NAO affects the subtropical high-pressure system and the associated low-level winds, which modulate the latent heat surface fluxes in the TNA and in the midlatitude North Atlantic region as proposed by *Cayan* [1992] and *Czaja et al.* [2002]. As a result, positive (negative) SST anomalies are established in the TNA and the Intertropical Convergence Zone (ITCZ), the main system modulating the northern NEB rainfall, located more to the north (south) than its normal position, thus creating favorable conditions to reduce (increase) rainfall over the northern NEB. These results also suggest that the relationship of the SLP variations in the NAO region and the NEB rainfall proposed by *Namias* [1972] is part of the decadal climate variability that connects the PDO in the tropical Pacific to the NEB rainfall through the NH midlatitudes. On the other hand, the positive correlation between the T-TSA and PRP indices implies that the negative (positive) SST anomalies in the TSA and the associated low-level winds are associated with the ITCZ located more to the north (south) than its normal position. These conditions favor drier (wetter) than normal conditions in the northern NEB.

[30] The relations of the SST (SLP) anomalies in the TSA to the northern NEB rainfall are weakly affected by the SST variations in the eastern Pacific and in the TNA and by the SLP variations in the NAO region for the decadal scale. On the other hand, the relations of the SST anomalies in the eastern Pacific and in the TNA to the northern NEB rainfall are also weakly influenced by the SST anomalies in the TSA. So the relations of the SST and SLP anomalies in the TSA to the NEB rainfall are mostly independent of the SST and SLP variability in the eastern Pacific and in the TNA, for the decadal scale. On the other hand, the SST and SLP variability in the eastern Pacific, in the NAO region, and in the TNA area is closely related to each other.

[31] The independent role of the TSA on the NEB rainfall is probably a further indication of the independent SST variability in both sides of the tropical Atlantic suggested by several authors [e.g., *Houghton and Tourre*, 1992; *Rajagopalan et al.*, 1998]. *Mélice and Servain* [2003] found separated SST modes in the TNA and the TSA with strong decadal component of distinct peridiodicity of 9.6 and 14 years, respectively. In this context, *Andreoli and Kayano* [2004], performing the wavelet analyses of the same SST indices for the TNA and the TSA used here, found dominant decadal peaks at 9.8 years for the T-TNA and at 12.7 years for the T-TSA. It is worth recalling that the global wavelet spectra (GWS) of the NEB and PRP indices (section 3.2) show a decadal peak at 12 years. Thus this decadal peak for the northern NEB rainfall indices is likely to reflect mostly the SST variability in the TSA. In summary, the results here suggest that the decadal variability of the northern NEB rainfall may be independently linked to the PDO/NAO/TNA decadal relations or to the SST decadal variations in the TSA.

[32] **Acknowledgments.** The authors are grateful to the two anonymous reviewers for their useful comments and suggestions. The authors were partially supported by the Conselho Nacional de Desenvolvimento Científico and Tecnológico of Brazil. Wavelet software was kindly provided by C. Torrence and G. Compo and is available at the URL http://paos.colorado.edu/research/wavelets. Thanks are also due to the UK Meteorological Office (UKMO) for providing the sea level pressure data used in this paper.

References

Aceituno, P. (1988), On the functioning of the Southern Oscillation in the South American sector. Part 1: Surface climate, *Mon. Weather Rev.*, *116*, 505–524.

Andreoli, R. V., and M. T. Kayano (2003), Evolution of the equatorial and dipole modes of the sea surface temperature in the tropical Atlantic at decadal scale, *Meteorol. Atmos. Phys.*, *83*, 277–285.

Andreoli, R. V., and M. T. Kayano (2004), Multi-scale variability of the sea surface temperature in the tropical Atlantic, *J. Geophys. Res.*, *109*, C05009, doi:10.1029/2003JC002220.

Cayan, D. (1992), Latent and sensible heat flux anomalies over the northern oceans: The connection to monthly atmospheric circulation, *J. Clim.*, *5*, 354–370.

Czaja, A., P. van der Vaart, and J. Marshall (2002), A diagnostic study of the role of remote forcing in tropical Atlantic variability, *J. Clim.*, *15*, 3280–3290.

Gershunov, A., and T. P. Barnett (1998), Interdecadal modulation of ENSO teleconnections, *Bull. Am. Meteorol. Soc.*, *79*, 2715–2725.

Häkkinen, S., and K. C. Mo (2002), The low-frequency variability of the tropical Atlantic Ocean, *J. Clim.*, *15*, 237–250.

Hastenrath, S. (1976), Variations in low-latitude circulation and extreme climatic events in the tropical Americas, *J. Atmos. Sci.*, *33*, 202–215.

Hastenrath, S., and L. Greischar (1993), Circulation mechanisms related to northeast Brazil rainfall anomalies, *J. Geophys. Res.*, *98*, 5093–5102.

Hastenrath, S., and L. Heller (1977), Dynamics of climatic hazards in northeast Brazil, *Q. J. R. Meteorol. Soc.*, *103*, 77–92.

Houghton, R. W., and Y. M. Tourre (1992), Characteristics of low-frequency sea surface temperature fluctuations in the tropical Atlantic, *J. Clim.*, *5*, 765–771.

Kane, R. P., and N. B. Trivedi (1988), Spectral characteristics of the annual rainfall series for northeast Brazil, *Clim. Change*, *13*, 317–336.

Kaplan, A., M. R. Cane, Y. Kushnir, A. C. Clement, M. B. Blumenthal, and B. Rajagopalan (1998), Analyses of global sea surface temperature 1856–1991, *J. Geophys. Res.*, *103*, 18,567–18,589.

Kayano, M. T., V. B. Rao, and A. D. Moura (1988), Tropical circulations and the associated rainfall anomalies during two contrasting years, *J. Climatol.*, *8*, 477–488.

Kiladis, G., and H. F. Diaz (1989), Global climatic anomalies associated with extremes in the Southern Oscillation, *J. Clim.*, *2*, 1069–1090.

Kousky, V. E., and P. S. Chu (1978), Fluctuations in annual rainfall for northeast Brazil, *J. Meteorol. Soc. Jpn.*, *56*, 457–466.

Kousky, V. E., and C. F. Ropelewski (1989), Extremes in the Southern Oscillation and their relationship to precipitation anomalies with emphasis on the South American region, *Rev. Bras. Meteorol.*, *4*, 351–363.

Kousky, V. E., M. T. Kayano, and I. F. A. Cavalcanti (1984), A review of the Southern Oscillation: Oceanic-atmospheric circulation changes and related rainfall anomalies, *Tellus, Ser. A*, *36*, 490–504.

Livezey, R. (1995), *Field Intercomparison, Analysis of Climate Variability*, edited by H. von Storch and A. Navarra, pp. 159–175, Springer-Verlag, New York.

Mantua, N. J., S. R. Hare, Y. Zhang, J. M. Wallace, and R. C. Francis (1997), A Pacific interdecadal climate oscillation with impacts on salmon production, *Bull. Am. Meteorol. Soc.*, *78*, 1069–1079.

Mehta, V. M. (1998), Variability of the tropical ocean surface temperatures at decadal-multidecadal timescales. Part I: The Atlantic Ocean, *J. Clim.*, *11*, 2351–2375.

Mehta, V. M., and T. Delworth (1995), Decadal variability of the tropical Atlantic Ocean surface temperature in shipboard measurements and in a global ocean-atmosphere model, *J. Clim.*, *8*, 172–190.

Mélice, J.-L., and J. Servain (2003), The tropical Atlantic meridional SST gradient index and its relationships with the SOI, NAO and Southern Ocean, *Clim. Dyn.*, *20*, 447–464.

Mo, K. C., and S. Häkkinen (2001), Decadal variations in the tropical South Atlantic and linkages to Pacific, *Geophys. Res. Lett.*, *28*, 2065–2068.

Moura, A. D., and J. Shukla (1981), On the dynamics of droughts in northeast Brazil: Observations, theory and numerical experiments with a general circulation model, *J. Atmos. Sci.*, *38*, 2653–2675.

Namias, J. (1972), Influence of Northern Hemisphere general circulation on drought in northeast Brazil, *Tellus*, *4*, 336–342.

Nitta, T., and S. Yamada (1989), Recent warming of tropical sea surface temperature and its relationship to the Northern Hemisphere circulation, *J. Meteorol. Soc. Jpn.*, *67*, 375–383.

Nobre, P., and J. Shukla (1996), Variations of sea surface temperature, wind stress and rainfall over the tropical Atlantic and South America, *J. Clim.*, *9*, 2464–2479.

Panofsky, H. A., and G. W. Brier (1968), *Some Applications of Statistics to Meteorology*, 224 pp., Pa. State Univ., University Park, Pa.

Rajagopalan, B., Y. Kushnir, and Y. M. Tourre (1998), Observed decadal midlatitude and tropical Atlantic climate variability, *Geophys. Res. Lett.*, *25*, 3967–3970.

Rao, V. B., and J. I. B. Brito (1985), Teleconnections between the rainfall over northeast Brazil and the winter circulation of Northern Hemisphere, *Pure Appl. Geophys.*, *123*, 951–959.

Rao, V. B., and K. Hada (1990), Characteristics of rainfall over Brazil: Annual variations and connections with the Southern Oscillation, *Theor. Appl. Climatol.*, *42*, 81–91.

Rogers, J. C. (1984), The association between the North Atlantic Oscillation and the Southern Oscillation in the Northern Hemisphere, *Mon. Weather Rev.*, *112*, 1999–2015.

Ropelewski, C. F., and M. S. Halpert (1987), Global and regional scale precipitation patterns associated with the El Niño/Southern Oscillation, *Mon. Weather Rev.*, *115*, 1606–1626.

Ropelewski, C. F., and M. S. Halpert (1989), Precipitation patterns associated with the high index phase of the Southern Oscillation, *J. Clim.*, *2*, 268–284.

Strang, D. M. G. D. (1972), Análise climatológica das normais pluviométricas do Nordeste Brasileiro (Climatological analysis of rainfall normals in the northeast Brazil), *Relat. Téc. IAE-M-02/72*, 70 pp., Cent. Téc. Aeroesp., São José dos Campos, São Paulo, Brazil.

Tanimoto, Y., and S.-P. Xie (1999), Ocean-atmosphere variability over the pan-Atlantic basin, *J. Meteorol. Soc. Jpn.*, *77*, 31–46.

Torrence, C., and G. P. Compo (1998), A practical guide to wavelet analysis, *Bull. Am. Meteorol. Soc.*, *79*, 61–78.

Tourre, Y. M., B. Rajagopalan, and Y. Kushnir (1999), Dominant patterns of climate variability in the Atlantic Ocean during the last 136 years, *J. Clim.*, *12*, 2285–2299.

Walker, G. T., and E. W. Bliss (1932), World weather V, *Mem. R. Meteorol. Soc.*, *4*, 53–84.

Wallace, J. M., and D. S. Gutzler (1981), Teleconnections in the geopotential height field during the Northern Hemisphere winter, *Mon. Weather Rev.*, *109*, 784–812.

Xie, S.-P., and Y. Tanimoto (1998), A pan-Atlantic decadal climate oscillation, *Geophys. Res. Lett.*, *25*, 2185–2188.

Zhang, C., and H. H. Hendon (1997), Propagating and standing components of the intraseasonal oscillation in tropical convection, *J. Atmos. Sci.*, *54*, 741–752.

Zhang, Y., J. M. Wallace, and D. Battisti (1997), ENSO-like interdecadal variability: 1900–93, *J. Clim.*, *10*, 1004–1020.

Zhang, Y., J. Norris, and J. M. Wallace (1998), Seasonality of large-scale atmosphere-ocean interaction over the North Pacific, *J. Clim.*, *11*, 2473–2481.

R. V. Andreoli and M. T. Kayano, Centro de Previsao de Tempo e Estudos Climaticos, Instituto Nacional de Pesquisas Espaciais, Av. dos Astronautas, 1758, São Jose dos Campos, São Paulo, 12227-010, Brazil. (mary@cptec.inpe.br)